Published in final edited form as:
Acta Biomater. 2013 April ; 9(4): 6268–6277. doi:10.1016/j.actbio.2012.12.002.

The Roles of Titanium Surface Micro/Nanotopography and Wettability on the Differential Response of Human Osteoblast Lineage Cells

Rolando A. Gittens[1,2], **Rene Olivares-Navarrete**[3], **Alice Cheng**[3], **David M. Anderson**[4,5], **Taylor McLachlan**[1], **Ingrid Stephan**[6], **Jürgen Geis-Gerstorfer**[6], **Kenneth H. Sandhage**[1,2,7], **Andrei G. Fedorov**[2,4,5], **Frank Rupp**[6], **Barbara D. Boyan**[1,2,3], **Rina Tannenbaum**[8], and **Zvi Schwartz**[2,3,9]

[1]School of Materials Science and Engineering, Georgia Institute of Technology, Atlanta, Georgia, USA

[2]Parker H. Petit Institute for Bioengineering and Bioscience, Georgia Institute of Technology, Atlanta, Georgia, USA

[3]Wallace H. Coulter Department of Biomedical Engineering at Georgia Tech and Emory University, Georgia Institute of Technology, Atlanta, GA, USA

[4]G.W. Woodruff School of Mechanical Engineering, Georgia Institute of Technology, Atlanta, Georgia, USA

[5]Institute of Paper Science and Technology, Georgia Institute of Technology, Atlanta, Georgia, USA

[6]Department of Prosthetic Dentistry, Section Medical Materials and Technology, University Hospital Tübingen, Tübingen, Germany

[7]School of Chemistry and Biochemistry, Georgia Institute of Technology, Atlanta, Georgia, USA

[8]Department of Biomedical Engineering, The School of Medicine and the UAB Comprehensive Cancer Center, University of Alabama at Birmingham, Birmingham, Alabama, USA

[9]Department of Periodontics, University of Texas Health Science Center at San Antonio, San Antonio, TX, USA

Abstract

Surface micro and nanostructural modifications of dental and orthopaedic implants have shown promising *in vitro*, *in vivo*, and clinical results. Surface wettability has also been suggested to play an important role in osteoblast differentiation and osseointegration. However, the available techniques to measure surface wettability are not reliable on clinically-relevant, rough surfaces. Furthermore, how the differentiation state of osteoblast lineage cells impacts their response to micro/nanostructured surfaces, and the role of wettability on this response, remains unclear. In the current study, surface wettability analyses (optical sessile drop analysis, ESEM analysis, and the

Address for Correspondence: Barbara D. Boyan, Ph.D., Institute for Bioengineering and Bioscience, Georgia Institute of Technology, 315 Ferst Drive, NW (Suite 1108), Atlanta, GA 30332-0363, Phone: 404-385-4108, FAX: 404-894-2291, barbara.boyan@bme.gatech.edu.

Wilhelmy technique) indicated hydrophobic static responses for deposited water droplets on microrough and micro/nanostructured specimens, while hydrophilic responses were observed with dynamic analyses of micro/nanostructured specimens. The maturation and local factor production of human immature osteoblast-like MG63 cells was synergistically influenced by nanostructures superimposed onto microrough titanium (Ti) surfaces. In contrast, human mesenchymal stem cells (MSCs) cultured on micro/nanostructured surfaces in the absence of exogenous soluble factors, exhibited less robust osteoblastic differentiation and local factor production compared to cultures on unmodified microroughened Ti. Our results support previous observations using Ti6Al4V surfaces showing that recognition of surface nanostructures and subsequent cell response is dependent on the differentiation state of osteoblast lineage cells. The results also indicate that this effect may be partly modulated by surface wettability. These findings support the conclusion that the successful osseointegration of an implant depends on contributions from osteoblast lineage cells at different stages of osteoblast commitment.

Keywords

commercially pure grade 2 titanium implants; osseointegration; bone; nanostructures; mesenchymal stem cell differentiation; dynamic contact angle

1. INTRODUCTION

While implants can provide important solutions to dental and orthopaedic problems, they still have undesirable failure rates in patients who are compromised by disease or age [1, 2]. Titanium (Ti) is widely used for implant applications due to its favorable weight-to-strength ratio and good biological performance in bone, which is intimately dependent on surface properties such as surface roughness, chemistry and wettability. Surface topographical modifications at the micrometer scale, such as are induced by acid etching and sandblasting, have been used effectively to enhance osteoblastic lineage cell differentiation *in vitro* [3, 4], and osseointegration *in vivo* [5] and clinically [6] compared to smoother surfaces. Recently, the addition of nanostructures to the surface of implants, to better mimic the hierarchical structure of bone, has also shown promising results *in vitro* [7], *in vivo* [8] and in the clinic [9, 10], which validates the biological relevance of nanotopography for bone formation.

Surface wettability can also influence implant osseointegration, with hydrophilic surfaces promoting an environment conducive to bone formation, as evidenced by enhanced osteoblast maturation *in vitro* [11, 12] and improved clinical success rates [13]. Certain surface treatments on clinically-available implants, such as microroughening and sterilization, can render surfaces hydrophobic due to adsorption of hydrocarbons and other contaminants [14, 15]. This can delay the initial interactions between the implant and the biological milieu, thereby impacting the subsequent cellular responses [16, 17].

The most common techniques to measure surface wettability (*i.e.*, optical sessile-drop contact angle measurements) were devised for smooth samples and only provide a static and approximate evaluation for microrough, clinically-relevant surfaces [18, 19] (Fig. 1A). Other factors that complicate the sessile-drop technique include variability in the chemistry of the wetting liquid and in the drop volume and size, as well as changes in vapor pressure and evaporation with temperature and time [18, 20]. Advancing and receding angles can be obtained with goniometers used for sessile-drop analyses; however, the dynamic information that can be extracted from the tilting of the stage is rather limited.

Other contact angle analyses have been developed to obtain a better representation of the true nature of the wettability of surfaces with complex topography. The environmental

scanning electron microscope (ESEM) provides enhanced spatial resolution and an environment with controlled pressure, temperature and humidity for microscale assessment of contact angle during nucleation, growth and coalescence of condensed droplets. ESEM imaging of water condensation can help minimize confounding results by avoiding air entrapment between microscale surface roughness features, which may make the surface appear more hydrophobic [21, 22] (Fig. 1B). Dynamic contact angle analysis using the Wilhelmy plate technique, in which a specimen is immersed into a known liquid using a tensiometer to measure the balancing forces, can also be used for the comprehensive assessment of surface wettability on non-ideal surfaces [23, 24] (Fig. 1C, D).

A recent study by our lab demonstrated that osteoblast-like MG63 cell maturation and local factor production was synergistically enhanced when exposed to oxidation-induced nanostructures superimposed on the surface of microrough Ti specimens [25]. Relatively high densities of nanostructures with SEM-derived diameters and heights ranging from 40 to 360 nm and 60 to 350 nm, respectively, were generated uniformly over the surface of Ti specimens using a heat treatment modification for 90 minutes. The short-lived surface oxidation caused by the heat treatment resulted in the growth of a 1.2 μm-thick compact and conformal oxide layer, with a diffraction pattern consistent with the presence of only the rutile polymorph of TiO_2, that lead to the nanostructuring of the surface. Surface analysis of the nanomodified specimens revealed that other surface characteristics, such as microroughness and wettability, as evaluated by the sessile-drop technique, were not affected by the oxidation treatment, leading to the conclusion that the addition of nanostructures was mainly responsible for the enhanced osteoblast response. However, experimental observations during the preparation of the specimens for contact angle analyses suggested that the dynamic behavior of the wettability of original and nanomodified specimens might be different (i.e., water droplets would easily roll off microrough surfaces, while the droplets had to be removed with compressed nitrogen from the surface of micro/nanostructured specimens), which could have an influence on the observed osteoblast response.

Mesenchymal stem cells (MSCs) and osteoprogenitor cells operate *in vivo* as initial colonizers of an implant surface due to their ability to migrate on osteoconductive surfaces of titanium implants [26], but comparatively little is known concerning their osteoblastic differentiation in response to implant surface properties, including nanotopography and wettability [27]. We have recently demonstrated that human MSCs can differentiate into osteoblasts when cultured on Ti surfaces possessing microscale roughness, even in the absence of osteogenic media supplements [28]. In the same study, it was found that MSCs could react synergistically to surface hydrophilicity when cultured on microrough surfaces. However, it is not known if osteoblastic differentiation of MSCs is a general response to microrough surfaces or if it can be affected by the superposition of nanoscale features, nor is it clear that surface wettability is involved in this response.

The goal of the present study was to test the hypothesis that nanostructural features on implant surfaces can affect the dynamic wettability of microrough Ti specimens, and that such surface property changes can, in turn, modulate the osteoblastic differentiation of osteoblast lineage cells in the absence of any exogenous soluble factors. To test this hypothesis, we superimposed nanostructures on clinically-relevant, microrough Ti surfaces and examined the responses of osteoblast-like MG63 cells and human MSCs without the addition of exogenous soluble osteogenic factors.

2. MATERIALS AND METHODS

2.1. Titanium Specimens and Surface Modification Treatments

Commercially pure Ti specimens (ASTM F67 unalloyed Ti grade 2 for surgical implant applications, sheet stock) with a cylindrical (15 mm in diameter, 1 mm thick) or rectangular ($20 \times 10 \times 1$ mm^3) shape were treated as described previously [11], to produce machined and pickled "pre-treatment" disks that were relatively smooth (referred to herein as PT specimens), and microrough "sandblasted-large-grit-acid-etched" disks (referred to herein as SLA specimens). All specimens were supplied by Institut Straumann AG (Basel, Switzerland).

Some of the microsmooth (PT) and microrough (SLA) specimens were further processed using a simple oxidation treatment to superimpose nanostructures on the surface, as described previously [25], to yield nanomodified, microsmooth (NMPT) or nanomodified, microrough (NMSLA) specimens. This oxidation treatment consisted of exposing the samples to flowing (0.85 standard liters per minute) synthetic air (21 % O_2, 79 % N_2) at 1 atm and 740 °C for 90 minutes [25]. All modified and unmodified disks were ultrasonically cleaned in detergent (Micro-90; International Products Corporation, Burlington, NJ) and ultrapure water (Advantage A10; Millipore, Billerica, MA), followed by autoclave sterilization (Model 2540E; Tuttnauer, Hauppauge, NY) for 20 minutes at 121 °C and 15 PSI before use. Surface characterization and cell culture studies, described below, focused on clinically-relevant, microrough specimens SLA and NMSLA, while microsmooth specimens (PT, NMPT) were used only as reference surfaces for topographical studies of the nanomodification and cell studies.

2.2. Surface Characterization

2.2.1. Electron Microscopy—Surface topography was qualitatively evaluated using a field-emission-gun scanning electron microscope (Ultra 60 FEG-SEM; Carl Zeiss SMT Ltd., Cambridge, UK). Secondary electron (SE) images were recorded using a 5 kV accelerating voltage and 30 μm aperture.

2.2.2. Atomic Force Microscopy (AFM)—Surface measurements at the nanoscale were evaluated using AFM (Nano-R AFM; Pacific Nanotechnology, Santa Clara, CA) in close-contact mode. Analyses were conducted using silicon probes (P-MAN-SICC-O, Agilent Technologies, Santa Clara, CA) with dimensions of 1.14 cm × 0.25 cm^2 and tip radii of up to 10 nm, a nominal force constant of 40 N/m, and a nominal resonance frequency of 300 kHz. Microsmooth specimens were used for AFM analyses due to a z-height limit of 5 μm for the AFM, which was less than the feature size of the microrough surfaces. Each AFM analysis was performed over a 730 nm × 730 nm specimen area. Two samples of each type of microsmooth specimen were scanned three times each, under ambient atmosphere. The raw data were plane-leveled to remove tilt by applying a numerical second-order correction, and mean values of surface roughness (S_a) were determined using NanoRule+ software (Pacific Nanotechnology).

2.2.3. Laser Confocal Microscopy (LCM)—Surface roughness at the microscale was evaluated using a laser confocal microscope (Lext LCM; Olympus, Center Valley, PA). Each LCM analysis was performed over a 644 μm × 644 μm area using a scan height step of 100 nm, a 20X objective, and a cutoff wavelength of 100 μm. Two samples of every specimen type were scanned three times each under ambient atmosphere. Mean values of the height parameter surface roughness average (S_a), and the spatial parameter texture aspect ratio (S_{tr}) were determined.

2.2.4. X-ray Photoelectron Spectroscopy (XPS)—Relative atomic concentration and chemical bonding information were obtained from the specimen surfaces by XPS analyses (Thermo K-Alpha XPS; Thermo Fisher Scientific, West Palm Beach, FL). The XPS instrument was equipped with a monochromatic Al-Kα X-ray source ($h\nu$ = 1468.6 eV). The XPS analysis chamber was evacuated to a pressure of 5×10^{-8} mbar or lower before collecting XPS spectra. Spectra were collected using an X-ray spot size of 400 μm and pass energy of 100 eV, with 1 eV increments, at a 55 ° takeoff angle. Two specimens of the SLA and NMSLA groups were scanned three times each and all values were averaged.

2.2.5. Sessile-Drop Contact Angle Measurements—Contact angle measurements were obtained using a drop shape analysis system (DSA 10-MK 2; Kruess, Hamburg, Germany) equipped with an automated stage and droplet dispenser, a digital camera, and image analysis software. Ultra-pure water (Simplicity 185 UV; Millipore, Billerica, MA), with water resistivity of 18.2 MΩ·cm at 25 °C, was used as the wetting liquid with a drop size of 5 μL (Fig. 1A). Sessile drop contact angles of the air-water-substrate interface were measured three times each on two samples from each specimen type.

2.2.6. Environmental Scanning Electron Microscope (ESEM) Contact Angle Analyses—Contact angle measurements at the micrometer level were assessed with an ESEM system (Quanta 200; FEI, Hillsboro, OR). Samples were placed directly onto a Peltier cooler (C2-08-0401; Tellurex, Traverse City, MI) in the ESEM chamber using a thin layer of thermal grease to ensure good thermal contact. The samples were oriented vertically, such that the electron beam was incident almost parallel to the surface, providing a side view of a droplet to assess contact angle. Imaged droplets were kept small relative to the capillary length of water (≪ 2 mm) such that surface tension forces were dominant over gravitational forces. The chamber was evacuated and then backfilled with pure deionized water vapor to a pressure of 773 Pa. To generate condensed water droplets on the surface, power was supplied to the Peltier cooler to cool the surface temperature below the saturation temperature of 4 °C at 773 Pa (Fig. 1B). The condensation of droplets on the surface was recorded and contact angles of the right-side interface of at least 10 droplets per image were calculated using image analysis software (ImageJ; NIH Software).

2.2.7. Dynamic Contact Angle (DCA) Analyses—Wettability and contact angle hysteresis were tensiometrically examined by the Wilhelmy method using an electrobalance (Sigma 70; Attension/KSV Instruments, Ltd., Espoo, Finland), as described previously [29]. Briefly, this technique uses a tensiometer to measure small changes in the forces (i.e. weight, buoyancy, and surface tension forces) exerted on a specimen of known size that is immersed in a reservoir of controlled liquid (Fig. 1C). The force balance equation is as follows:

$$F = M \cdot g - \rho \cdot g \cdot t \cdot H \cdot d + L \cdot \gamma_L \cdot \cos\theta \quad (1)$$

where F is the total force exerted on the sample, M is the mass of the plate, g is the gravitational acceleration, is the liquid density, t is the thickness of the plate, H is the width of the plate, d is the immersion-emersion depth, L is the plate perimeter [$L = 2\ (t+H)$], γ_L is the liquid surface tension, and is the contact angle at the liquid-solid-vapor interface. By setting the balance (*i.e.*, weight of the specimen) to zero before each run and using a linear regression to zero for the immersion-emersion depth, the first two terms of equation (1) are cancelled and the contact angle can be calculated directly from the force measured by the tensiometer.

Ultra-pure water was selected as the liquid phase for the experiments, and the specimens were immersed and then emerged at a speed of 10 mm/min for a depth of 10 mm for 10

cycles using a motorized water reservoir (Figs. 1C and D). Once the meniscus had formed, the contact angle was assumed to remain constant throughout the immersion-emersion loop. Contact angle calculations were performed ignoring the initial 6 mm of immersion or emersion from each loop. All measurements were performed at room temperature in an environment with controlled temperature (23 °C) and relative humidity (35 %). Two samples of each specimen group were analyzed. For one of the studies, the autoclave-sterilized SLA specimens that had been analyzed by DCA were subsequently cleaned using ultrasonication in ultra-pure water for 15 minutes and dried for 2 hours under vacuum using a vacuum pump (Trivac D4B; Oerlikon Leybold Vacuum GmbH, Koeln, Germany). These specimens were used again for DCA analyses to determine whether the surface response to the immersion-emersion loops was permanent or dependent on physisorbed molecules.

2.3. Cell Culture Model

Human osteoblast-like MG63 cells and human mesenchymal stem cells (MSCs) were used for this study. MG63 cells were obtained from the American Type Culture Collection (Rockville, MD) and were cultured in Dulbecco's modified Eagle medium (DMEM cellgro®; Mediatech, Inc., VA) containing 10 % fetal bovine serum (FBS; Gibco, Carlsbad, CA) and 1 % penicillin-streptomycin. Human MSCs were purchased from a commercial vendor (Lonza, Walkersville, MD) and grown in MSC Growth Medium (MSCGM; Lonza). All cells were cultured at 37 °C with 5 % CO_2 and 100 % humidity. MG63s and MSCs were cultured on tissue culture polystyrene (TCPS) to check for confluence, on PT surfaces as a control, or on the different microrough, clinically-relevant surfaces (SLA, NMSLA) at a seeding density of 10,000 cells/cm^2. Seeding density was normalized to the area of the disk in order to use the same initial seeding density on all substrates and evaluate the effect of surface topography on similar cell populations. Cells were fed 24 hours after plating, and then every 48 hours until confluence, as evaluated on the TCPS substrates. At confluence, cells were incubated with fresh medium for 24 hours and harvested for assays. Conditioned media were collected and stored at −80 °C until assayed. Cell layers were washed twice with serum-free medium and released from their substrate by two sequential incubations in 500 μL 0.25 % trypsin for 10 minutes at 37 °C. Cells were resuspended in 500 μL 0.05 % Triton-X-100® and lysed by sonication. MG63 cell number was evaluated by measuring DNA content with a commercially-available kit (Quant-iT™ PicoGreen® dsDNA assay; Invitrogen, Carlsbad, CA) and a fluorescent multimode detector (DTX880; Beckman Coulter, Brea, CA) with reference to a standard. MSCs were counted, before cell lysis, with a Z1 Coulter particle counter (Beckman Coulter, Brea, CA).

Osteoblastic differentiation was evaluated by measuring the osteocalcin content in the conditioned media as a late differentiation marker. Osteocalcin was measured using a commercially-available radioimmunoassay kit (Human Osteocalcin RIA Kit; Biomedical Technologies, Stoughton, MA) as described previously [30], using a LS1500 gamma counter (Perkin Elmer, Waltham, CA). The conditioned media were also assayed for protein levels of local factors important for bone development. Osteoprotegerin (OPG), a cytokine that works as a decoy receptor for "receptor activator for nuclear factor B ligand" (RANKL) to inhibit osteoclastogenesis, was measured using enzyme-linked immunosorbent assay (ELISA) kits (DY805 Osteoprotegerin DuoSet; R&D Systems, Minneapolis, MN). Vascular endothelial growth factor (VEGF), a growth factor involved in vasculogenesis and angiogenesis, was also measured using an ELISA kit (DY293B VEGF DuoSet; R&D Systems).

2.4. Statistical Analyses

Data from experiments evaluating the surface characteristics of the substrates are presented as the mean ± one standard deviation (SD) of all the measurements performed on different

samples of the same specimen type. Data from experiments examining cell response are presented as the mean ± standard error (SE) of the treatment (SLA, NMSLA) over control (PT) for two experiments with six independent cultures per variable. All experiments were repeated at least twice to ensure reproducibility. Data were evaluated by analysis of variance, and significant differences between groups were determined using Student's t-test. A p value below 0.05 was considered to indicate a statistically-significant difference.

3. RESULTS

3.1. Characterization of Nanomodified Surfaces

Secondary electron images of the original SLA surfaces revealed peaks and valleys on the order of tens of micrometers as a result of the sandblasting process, with additional sharp sub-microscale features left from the acid-etch treatment (Fig. 2A). The surface of the microrough specimens that had received the 740 °C oxidation treatment for 90 minutes (NMSLA) possessed high and homogeneous concentrations of nanostructures (Fig. 2B). The qualitative increase in the nanoscale roughness of the Ti surfaces detected by electron microscopy after the oxidation treatment was confirmed by AFM analyses (Fig. 3), which revealed significant enhancements in the values of the mean nanoscale roughness average. As expected, roughness average measured by laser confocal microscopic analyses revealed that the microroughness of the SLA and NMSLA specimens was significantly higher than for the pre-treatment specimens (PT and NMPT) (Fig. 3). In addition, surface microroughness, as determined by average roughness (S_a, Fig. 3) and texture aspect ratio (S_{tr}, Suppl. Table 1), was not noticeably affected by the superposition of surface nanostructures during the subsequent oxidation treatment.

The addition of nanoscale features to microrough SLA surfaces by oxidation heat treatment altered the surface chemistry of the specimens (Fig. 4). The elemental compositions of both the original SLA and nanomodified NMSLA surfaces after autoclave sterilization included the same elements, Ti, atomic oxygen (O) and carbon (C), as the major components. However, the oxidation treatment altered the concentrations of these elements on the surface, with a significant reduction in C and significantly higher concentrations of Ti and O on the oxidized surfaces than for the microrough specimens. Small concentrations of nitrogen (N) were also present on the original SLA surfaces, while only traces were found on the NMSLA surfaces. In addition, traces of impurities such as calcium (Ca) and chlorine (Cl) were found on the SLA specimens, which were not detectable on NMSLA specimens.

Values obtained for the water contact angles for microrough and nanomodified Ti specimens were dependent on the measurement method. Optical sessile-drop contact angle analysis conducted in air, a technique commonly used to indirectly assess the relative surface energy of biomaterials, showed that autoclave-sterilized SLA and NMSLA specimens exhibited strong hydrophobic responses to water (Fig. 5A). However, in some cases the water droplet could not be dispensed on the surface of SLA specimens or would easily roll off, which was not observed for the NMSLA specimens. ESEM imaging in a pure water vapor atmosphere was used to evaluate the wetting behavior of condensed water droplets on the surfaces of the specimens at the micro scale. ESEM images revealed that the SLA and NMSLA specimens exhibited hydrophilic behavior with droplets having contact angles close to 50 °, whereas droplets that nucleated at length scales smaller than the roughness features exhibited complete wetting of the surface (Fig. 5B, Suppl. Video 1). There was no significant difference in wettability of the SLA and NMSLA surfaces as observed from ESEM analyses.

Dynamic contact angle analyses of the SLA and NMSLA surfaces using the Wilhelmy balance technique provided a quantitative assessment of wettability that differed from the

sessile drop measurements. Force graphs of 10-loop Wilhelmy experiments showed extremely negative F/L values for the initial advancing loop of SLA (Fig. 5C) and NMSLA (Fig. 5D) specimens. Subsequent immersion-emersion loops on the SLA specimens continued to show negative values with hysteresis, and the sample did not reach equilibrium even after the 10^{th} loop. In contrast, NMSLA specimens presented more positive F/L values for all following loops without evidence of appreciable hysteresis. The sterilized SLA specimens that were ultrasonically cleaned and dried under vacuum after DCA and reanalyzed showed an initial loop with a slightly negative F/L value and more positive values for the subsequent loops with no appreciable hysteresis (Fig. 5E). Contact angles calculated from the measured F/L values (Fig. 6) indicated that the initial advancing angles of the autoclaved SLA and NMSLA specimens were hydrophobic and similar to the sessile-drop contact angle values. However, the second to tenth loops on the SLA specimens showed decreasing advancing angles that remained above 100 ° and receding angles that averaged around 70 °. In the case of NMSLA specimens, the second to tenth loops resulted in superhydrophilic advancing and receding contact angles of less than 10 °.

3.2. Osteoblast Lineage Cell Response to Nanomodified Surfaces

MG63 osteoblastic maturation was synergistically enhanced by the nanostructures superimposed onto microrough Ti surfaces, while MSC osteoblastic differentiation was suppressed by the same micro/nanostructured surfaces. Cell number (Fig. 7A), which decreases as cells transition from a proliferative to a more mature state, was lower for MG63s on the microrough surfaces compared to the microsmooth control, with the lowest levels on the combined microrough and nanostructured NMSLA surfaces. MSCs on microrough SLA surfaces also had lower numbers than controls, similar to MG63s on SLA, but the numbers were back to control levels on the NMSLA surfaces. At the same time, the production of the late osteoblastic differentiation marker osteocalcin (Fig. 7B) was higher for MG63s on the SLA group compared to controls and significantly higher on NMSLA surfaces. MSCs on SLA surfaces also had higher levels of osteocalcin compared to controls, with an increase in production similar to that of MG63s on SLA. Osteocalcin production by MSCs on SLA surfaces was also significantly higher than on NMSLA surfaces, with the latter being no different than controls.

Levels of the anti-osteoclastogenesis factor osteoprotegerin (Fig. 7C) and the angiogenic factor VEGF (Fig. 7D) were also evaluated in association to the differentiation of the cells. MG63s produced higher levels of osteoprotegerin and VEGF on both microrough groups compared to microsmooth controls, with the highest levels found on the combined micro/nanostructured NMSLA surfaces. Conversely, MSCs produced slightly lower levels of osteoprotegerin on the different microrough groups compared to controls, with the lowest levels found on the NMSLA specimens. Additionally, MSCs produced higher levels of VEGF on SLA surfaces compared controls, while the levels on NMSLA specimens were slightly lower than controls.

4. DISCUSSION

In this study, the cellular responses of progenitor cells and cells representative of an immature osteoblastic phenotype have been compared on clinically-relevant, microrough titanium (Ti) specimens before and after surface superposition of oxidation-induced nanostructures. Osteoblast maturation, as evaluated by the production of osteoblast differentiation markers and local factors that promote osteogenesis, was significantly enhanced by the addition of nanostructures to microrough surfaces. In contrast, our results suggest that MSC osteoblastic differentiation and local osteogenic factor production were suppressed on the combined micro/nanostructured surfaces, whereas MSC cell numbers were increased. These results indicate that osteoblast-lineage cell response to nanostructures

presented on the surface of microrough surfaces is dependent on their current differentiation state. Additionally, changes in surface wettability caused by the nanomodification may also be partly responsible for the cellular responses reported. These observations are discussed in detail below.

The heat treatment nanomodification recently developed by our group [25] was used to modify clinically-relevant, microrough Ti specimens. The treatment yielded a high density of nanostructural features on microrough surfaces, covering areas that would have been difficult to modify by line-of-sight sandblasting-based treatments (*i.e.,* standard treatments used for dental implant surfaces). Another attractive attribute of the oxidation-based treatment for the generation of nanostructures on Ti was that other surface characteristics, such as surface microroughness, remained constant, which allowed for reduced ambiguity in assessing the effect of the nanostructures on cell response.

Surface roughness evaluations at the nanoscale, as measured by AFM, quantitatively confirmed the presence of the nanostructures, while assessment by LCM showed no significant degradation in microroughness by the oxidation process, in agreement with our previous study [25]. The major elemental constituents on the surfaces were Ti, O, and C before and after the oxidation treatment, and following the cleaning and sterilization protocol. However, the concentrations of these elements were altered, with higher levels of Ti and O, and lower levels of C, on the nanomodified specimens. The surface concentrations of other impurities such as N, Ca, and Cl were also lower or nonexistent on the oxidized specimens. High levels of C on the surface of Ti specimens have been linked to hydrocarbon contamination during autoclave sterilization, which can also be responsible for the addition of other impurities such as N and Cl on the surfaces of Ti implants [15]. Interestingly, carbon content on NMSLA specimens before (data not shown) and after autoclaving were similar and comparable to that of SLA specimens before autoclaving, which generally present carbon content in the range of 25 to 35 % [12, 23]. We could speculate that the lower carbon content on the NMSLA specimens could be due to the oxide layer being hydroxilated after the heat treatment, leaving less exposed sites for hydrocarbon adsorption. Another possibility could be that the thicker oxide layer or the nanostructuring of the surface could interfere with the affinity and subsequent adsorption of hydrocarbons. Yet, we did not evaluate these possibilities in our experimental design as we considered them to be outside the scope of our study. Most commercially-available dental implants are currently sterilized by gamma irradiation; however, autoclave sterilization is still widely used for orthopaedic implants. The effect of these impurities on cell response remains unclear, but our results indicate that the oxidation-based generation of surface nanostructures on microrough Ti specimens acted to reduce the presence of hydrocarbons and other impurities.

Static assessment of the wettability of microrough and combined micro/nanostructured surfaces indicated that both groups had strong hydrophobic responses, as shown previously on these same specimens [25]. ESEM measurements can provide insights about the wettability responses of surfaces at the microscale, but still depend on the assessment of single droplets [22]. Microrough and micro/nanostructured specimens exhibited more hydrophilic contact angles when evaluated by ESEM analyses in pure water vapor, compared to optical sessile-drop analyses conducted in ambient air, which suggested that the hydrophobic effect observed by the latter technique could have been due to air trapped underneath the deposited droplet and that the Ti/TiO_2 surface possessed a hydrophilic nature in the absence of environmental contamination. Regardless, contact angle values obtained by each type of measurement were similar for the SLA and NMSLA specimens.

In contrast to static contact angle analyses, the dynamic behavior of the water/substrate interfaces revealed significant differences between the two types of samples. After

sterilization, the microrough specimens exhibited a strong hydrophobic response that did not reach equilibrium even after 10 immersion-emersion loops. The receding angles, which were lower than 90 ° and thus hydrophilic, were still relatively high. Interestingly, the unstable hydrophobic response of the sterilized microrough specimens could be eliminated by cleaning them in ultra-pure water, suggesting that the sustained hydrophobic response was due to physisorbed contaminants on the surface. After the initial hydrophobic loop for all of the autoclaved micro/nanostructured specimens, subsequent advancing and receding loops showed complete wettability. Previous studies on microrough-only specimens without autoclave sterilization showed an initial hydrophobic advancing loop, with subsequent advancing and receding angles reaching an extremely hydrophilic equilibrium [23]. The latter results are unlike what was observed in the present study for the sterilized microrough specimens, but are in agreement with our results on the cleaned, microrough specimens as well as on the micro/nanostructured specimens. Observations of droplets that rolled off easily from SLA specimens, but not from NMSLA specimens, were consistent with the very low receding angles on the NMSLA specimens which were apparently due to a strong surface/water interaction with NMSLA specimens during dewetting (recession). The present data suggest that autoclave sterilization can degrade the dynamic surface wettability response of microrough specimens, possibly due to physisorption of surface contaminants as detected by XPS. The oxidation-based nanomodification process can help maintain the hydrophilic dynamic behavior of the specimens, which may have an impact on cell response.

Osteoblasts responded synergistically to the combined micro/nanostructured surfaces in terms of maturation and local factor production, as reported in our previous study [25]. Lower osteoblast cell numbers were found on the microrough surfaces, with the lowest levels found on the combined microrough and nanostructured surfaces. In addition, synergistically higher production of the late differentiation marker osteocalcin was reported for the micro/nanostructured surfaces compared to controls and microrough specimens, indicating enhanced osteoblast maturation on these surfaces when taken together with the cell number results. Low cell number in combination with increased production of osteoblastic differentiation markers has been used previously to determine osteoblast maturation *in vitro* [31], in part due to a transcriptionally-restricted regulation between osteoblasts' proliferative and differentiating state [32]. Such osteoblast response is characteristic of microrough surfaces *in vitro* [33] and has been correlated to the successes of microrough surfaces relative to smoother surfaces *in vivo* [34] and in the clinic [35, 36]. Superposition of nanostructures on microrough surfaces also synergistically promoted the production of the anti-osteoclastogenic factor osteoprotegerin and the pro-angiogenic factor VEGF, as reported in our previous study using the same types of specimens [25]. Enhanced differentiation and higher production of local factors by osteoblasts have been reported for microrough surfaces with hydrophilic surfaces [16, 37], suggesting that the dynamic hydrophilic behavior of the micro/nanostructured specimens could be playing a role in the enhanced cell response.

MSC osteoblastic differentiation responded to microroughness, as seen previously [28], but did not react to nanostructures superimposed onto microrough Ti specimens. MSC numbers decreased on the microrough surfaces compared to the microsmooth controls, to similar levels seen in osteoblasts on these same surfaces. Furthermore, the production of osteocalcin was enhanced on the microrough specimens relative to controls, again to similar levels observed in osteoblasts on these microrough surfaces, confirming the influence of microroughness on the enhanced differentiation of MSCs [3, 28]. Conversely, MSC numbers and osteocalcin production on the micro/nanostructured surfaces were similar to control levels, suggesting that the differentiation of MSCs was suppressed by the superposition of nanostructures. Additionally, compared to the microrough-only surfaces,

the nanomodified microrough surfaces generated lower production of local factors associated with bone formation, osteoprotegerin and VEGF.

Our results fall in line with a recent study showing that polycaprolactone (PCL) surfaces with certain symmetric nanostructural features could promote MSC stemness *in vitro* without the use of any exogenous factors, as confirmed by lower production of the osteoblast markers osteocalcin and osteopontin as well as higher levels of the skeletal stem cell markers STRO-1 and ALCAM [38]. Although differences in the substrate characteristics between the studies does not allow for a direct comparison, the superposition of nanostructures on microrough Ti substrates still appeared to interfere with the osteoblastic differentiation of MSCs. MSCs are multipotent, thus it is possible that the nanotopography and wettability of the NMSLA surface elicited alternative lineage commitments. The fact that the cells were able to proliferate to the same extent as cells cultured on microsmooth control surfaces argues against quiescence being induced in the entire MSC population, although it is possible that the stemness property of a subset of cells was retained.

Other groups have reported enhanced osteoblastic differentiation of MSCs growing on micro/nanostructured surfaces [7, 39]. Nonetheless, the majority of these studies used exogenous factors that can force osteogenic differentiation of the stem cells, such as dexamethasone and β-glycerophosphate, effectively committing their MSCs to the osteoblast lineage and obscuring the real effects of the surface nanotopography. We observed that MG63 cells, which are immature osteoblasts, responded synergistically to the nanostructures on microrough Ti specimens with increased production of osteocalcin and other osteogenic proteins and this occurred even without the use of these soluble factors. This suggests that the state of maturation within the osteoblast lineage may determine that nature of the response to the material surface.

While surface micro/nanotopography is clearly a critical variable, variations in surface physicochemical properties are also important modulators of cell response. A previous study by our group showed enhanced osteoblastic differentiation by MSCs when grown on hydrophilic microrough Ti surfaces compared to hydrophobic specimens with the same topography [28], suggesting that the effect of superimposed nanostructures may play a more dominant role than wettability in the suppression of MSC osteoblastic differentiation found in the current study. The present results support recent observations by our group using Ti6Al4V surfaces showing that recognition of surface nanostructures, and subsequent cell response, is dependent on the differentiation state of osteoblast lineage cells [40].

5. CONCLUSIONS

Our results demonstrate that osteoblastic lineage cell fate can be modulated by controlling surface characteristics, such as nanotopography and wettability, without the use of exogenous soluble factors, and the corresponding response is dependent on the differentiation state of the cells. These findings support the conclusion that the successful osseointegration of an implant depends on different contributions from osteoblast lineage cells at different stages of osteoblast commitment. Nanostructures superimposed by oxidation onto microrough Ti surfaces, in the absence of any exogenous soluble factors, strongly enhanced the maturation of immature osteoblast-like cells, whereas the same surfaces suppressed MSC osteoblastic differentiation and osteogenic local factor production while supporting proliferation. Differences in the surface wettability introduced by the surface nanomodification may be partly responsible for the responses of osteoblast lineage cells.

Supplementary Material

Refer to Web version on PubMed Central for supplementary material.

Acknowledgments

This research was supported by USPHS AR052102 and the ITI Foundation. Partial support for the work of RAG was provided by a fellowship from the Government of Panama (IFARHU-SENACYT), as well as by the IMI Program of the National Science Foundation (ICMR Program, Award No. DMR04-09848). Support for the work of TM, YC, DMA and AGF was provided by the U.S. Air Force Office of Scientific Research (Award No. FA9550-09-1-0162). DMA is also supported by a PSE fellowship from the Georgia Tech Institute of Paper Science and Technology. Support for the work of KHS was provided by the U.S. Department of Energy, Office of Basic Energy Sciences (Award No. DE-SC0002245). The PT and SLA disks were provided by Institut Straumann AG (Basel, Switzerland).

References

1. Fransson C, Wennstrom J, Berglundh T. Clinical characteristics at implants with a history of progressive bone loss. Clin Oral Implants Res. 2008; 19:142–7. [PubMed: 18184340]
2. Granstrom G. Osseointegration in irradiated cancer patients: An analysis with respect to implant failures. J Oral Maxillofac Surg. 2005; 63:579–85. [PubMed: 15883929]
3. Wall I, Donos N, Carlqvist K, Jones F, Brett P. Modified titanium surfaces promote accelerated osteogenic differentiation of mesenchymal stromal cells in vitro. Bone. 2009; 45:17–26. [PubMed: 19332166]
4. Kim MJ, Kim CW, Lim YJ, Heo SJ. Microrough titanium surface affects biologic response in MG63 osteoblast-like cells. J Biomed Mater Res A. 2006; 79:1023–32. [PubMed: 17034031]
5. Buser D, Schenk RK, Steinemann S, Fiorellini JP, Fox CH, Stich H. Influence of surface characteristics on bone integration of titanium implants - A histomorphometric study in miniature pigs. J Biomed Mater Res. 1991; 25:889–902. [PubMed: 1918105]
6. Cochran DL, Jackson JM, Bernard JP, ten Bruggenkate CM, Buser D, Taylor TD, et al. A 5-year prospective multicenter study of early loaded titanium implants with a sandblasted and acid-etched surface. Int J Oral Maxillofac Implants. 2011; 26:1324–32. [PubMed: 22167440]
7. Mendonca G, Mendonca DBS, Aragao FJL, Cooper LF. The combination of micron and nanotopography by H2SO4/H2O2 treatment and its effects on osteoblast-specific gene expression of hMSCs. J Biomed Mater Res A. 2010; 94A:169–79. [PubMed: 20128007]
8. Tsukimura N, Ueno T, Iwasa F, Minamikawa H, Sugita Y, Ishizaki K, et al. Bone integration capability of alkali- and heat-treated nanobimorphic Ti-15Mo-5Zr-3Al. Acta Biomater. 2011; 7:4267–77. [PubMed: 21888994]
9. Orsini G, Piattelli M, Scarano A, Petrone G, Kenealy J, Piattelli A, et al. Randomized, controlled histologic and histomorphometric evaluation of implants with nanometer-scale calcium phosphate added to the dual acid-etched surface in the human posterior maxilla. J Periodontol. 2007; 78:209–18. [PubMed: 17274708]
10. Collaert B, Wijnen L, De Bruyn H. A 2-year prospective study on immediate loading with fluoride-modified implants in the edentulous mandible. Clin Oral Implants Res. 2011; 22:1111–6. [PubMed: 21244503]
11. Zhao G, Schwartz Z, Wieland M, Rupp F, Geis-Gerstorfer J, Cochran DL, et al. High surface energy enhances cell response to titanium substrate microstructure. J Biomed Mater Res. 2005; 74A:49–58.
12. Park JH, Wasilewski CE, Almodovar N, Olivares-Navarrete R, Boyan BD, Tannenbaum R, et al. The responses to surface wettability gradients induced by chitosan nanofilms on microtextured titanium mediated by specific integrin receptors. Biomaterials. 2012; 33:7386–93. [PubMed: 22835642]
13. Bornstein MM, Wittneben JG, Bragger U, Buser D. Early loading at 21 days of non-submerged titanium implants with a chemically modified sandblasted and acid-etched surface: 3-year results of a prospective study in the posterior mandible. J Periodontol. 2010; 81:809–18. [PubMed: 20450357]

14. Park JH, Olivares-Navarrete R, Baier RE, Meyer AE, Tannenbaum R, Boyan BD, et al. Effect of cleaning and sterilization on titanium implant surface properties and cellular response. Acta Biomater. 2012; 8:1966–75. [PubMed: 22154860]
15. Lausmaa J. Surface spectroscopic characterization of titanium implant materials. J Electron Spectrosc Relat Phenom. 1996; 81:343–61.
16. Park JH, Olivares-Navarrete R, Wasilewski CE, Boyan BD, Tannenbaum R, Schwartz Z. Use of polyelectrolyte thin films to modulate Osteoblast response to microstructured titanium surfaces. Biomaterials. 2012; 33:5267–77. [PubMed: 22541354]
17. Ferguson SJ, Broggini N, Wieland M, de Wild M, Rupp F, Geis-Gerstorfer J, et al. Biomechanical evaluation of the interfacial strength of a chemically modified sandblasted and acid-etched titanium surface. J Biomed Mater Res A. 2006; 78A:291–7. [PubMed: 16637025]
18. Good RJ. Contact-angle, wetting, and adhesion - a critical-review. J Adhes Sci Technol. 1992; 6:1269–302.
19. Watanabe T. Wettability of ceramic surfaces -A wide range control of surface wettability from super hydrophilicity to super hydrophobicity, from static wettability to dynamic wettability. J Ceram Soc Jpn. 2009; 117:1285–92.
20. Drelich J, Miller JD, Good RJ. The effect of drop (bubble) size on advancing and receding contact angles for heterogeneous and rough solid surfaces as observed with sessile-drop and captive-bubble techniques. J Colloid Interf Sci. 1996; 179:37–50.
21. Rykaczewski K, Scott JHJ, Fedorov AG. Electron beam heating effects during environmental scanning electron microscopy imaging of water condensation on superhydrophobic surfaces. Appl Phys Lett. 2011; 98:0931061–3.
22. Liukkonen A. Contact angle of water on paper components: Sessile drops versus environmental scanning electron microscope measurements. Scanning. 1997; 19:411–5.
23. Rupp F, Scheideler L, Olshanska N, deWild M, Wieland M, Geis-Gerstorfer J. Enhancing surface free energy and hydrophilicity through chemical modification of microstructured titanium implant surfaces. J Biomed Mater Res A. 2006; 76A:323–34. [PubMed: 16270344]
24. Rupp F, Scheideler L, Eichler M, Geis-Gerstorfer J. Wetting Behavior of Dental Implants. Int J Oral Maxillofac Implants. 2011; 26:1256–66. [PubMed: 22167431]
25. Gittens RA, McLachlan T, Olivares-Navarrete R, Cai Y, Berner S, Tannenbaum R, et al. The effects of combined micron-/submicron-scale surface roughness and nanoscale features on cell proliferation and differentiation. Biomaterials. 2011; 32:3395–403. [PubMed: 21310480]
26. Davies JE. In vitro modeling of the bone/implant interface. Anat Rec. 1996; 245:426–45. [PubMed: 8769677]
27. McNamara LE, Sjostrom T, Burgess KEV, Kim JJW, Liu E, Gordonov S, et al. Skeletal stem cell physiology on functionally distinct titania nanotopographies. Biomaterials. 2011; 32:7403–10. [PubMed: 21820172]
28. Olivares-Navarrete R, Hyzy SL, Hutton DL, Erdman CP, Wieland M, Boyan BD, et al. Direct and indirect effects of microstructured titanium substrates on the induction of mesenchymal stem cell differentiation towards the osteoblast lineage. Biomaterials. 2010; 31:2728–35. [PubMed: 20053436]
29. Rupp F, Axmann D, Ziegler C, Geis-Gerstorfer J. Adsorption/desorption phenomena on pure and Teflon((R)) AF-coated titania surfaces studied by dynamic contact angle analysis. J Biomed Mater Res. 2002; 62:567–78. [PubMed: 12221705]
30. Boyan BD, Batzer R, Kieswetter K, Liu Y, Cochran DL, Szmuckler-Moncler S, et al. Titanium surface roughness alters responsiveness of MG63 osteoblast-like cells to 1 alpha,25-(OH)(2)D-3. J Biomed Mater Res. 1998; 39:77–85. [PubMed: 9429099]
31. Lincks J, Boyan BD, Blanchard CR, Lohmann CH, Liu Y, Cochran DL, et al. Response of MG63 osteoblast-like cells to titanium and titanium alloy is dependent on surface roughness and composition. Biomaterials. 1998; 19:2219–32. [PubMed: 9884063]
32. Stein GS, Lian JB, Stein JL, VanWijnen AJ, Montecino M. Transcriptional control of osteoblast growth and differentiation. Physiol Rev. 1996; 76:593–629. [PubMed: 8618964]

33. Zinger O, Zhao G, Schwartz Z, Simpson J, Wieland M, Landolt D, et al. Differential regulation of osteoblasts by substrate microstructural features. Biomaterials. 2005; 26:1837–47. [PubMed: 15576158]
34. Buser D, Nydegger T, Oxland T, Cochran DL, Schenk RK, Hirt HP, et al. Interface shear strength of titanium implants with a sandblasted and acid-etched surface: a biomechanical study in the maxilla of miniature pigs. J Biomed Mater Res. 1999; 45:75–83. [PubMed: 10397960]
35. Bornstein MM, Schmid B, Belser UC, Lussi A, Buser D. Early loading of non-submerged titanium implants with a sandblasted and acid-etched surface. 5-year results of a prospective study in partially edentulous patients. Clin Oral Implants Res. 2005; 16:631–8. [PubMed: 16307568]
36. Cochran DL, Buser D, ten Bruggenkate CM, Weingart D, Taylor TM, Bernard JP, et al. The use of reduced healing times on ITI (R) implants with a sandblasted and acid-etched (SLA) surface: Early results from clinical trials on ITI (R) SLA implants. Clin Oral Implants Res. 2002; 13:144–53. [PubMed: 11952734]
37. Zhao G, Raines AL, Wieland M, Schwartz Z, Boyan BD. Requirement for both micron- and submicron scale structure for synergistic responses of osteoblasts to substrate surface energy and topography. Biomaterials. 2007; 28:2821–9. [PubMed: 17368532]
38. McMurray RJ, Gadegaard N, Tsimbouri PM, Burgess KV, McNamara LE, Tare R, et al. Nanoscale surfaces for the long-term maintenance of mesenchymal stem cell phenotype and multipotency. Nat Mater. 2011; 10:637–44. [PubMed: 21765399]
39. Khang D, Choi J, Im YM, Kim YJ, Jang JH, Kang SS, et al. Role of subnano-, nano- and submicron-surface features on osteoblast differentiation of bone marrow mesenchymal stem cells. Biomaterials. 2012; 33:5997–6007. [PubMed: 22632766]
40. Gittens RA, Olivares-Navarrete R, McLachlan T, Cai Y, Hyzy SL, Schneider JM, et al. Differential responses of osteoblast lineage cells to nanotopographically-modified, microroughened titanium-aluminum-vanadium alloy surfaces. Biomaterials. 2012; 33:8986–94. [PubMed: 22989383]

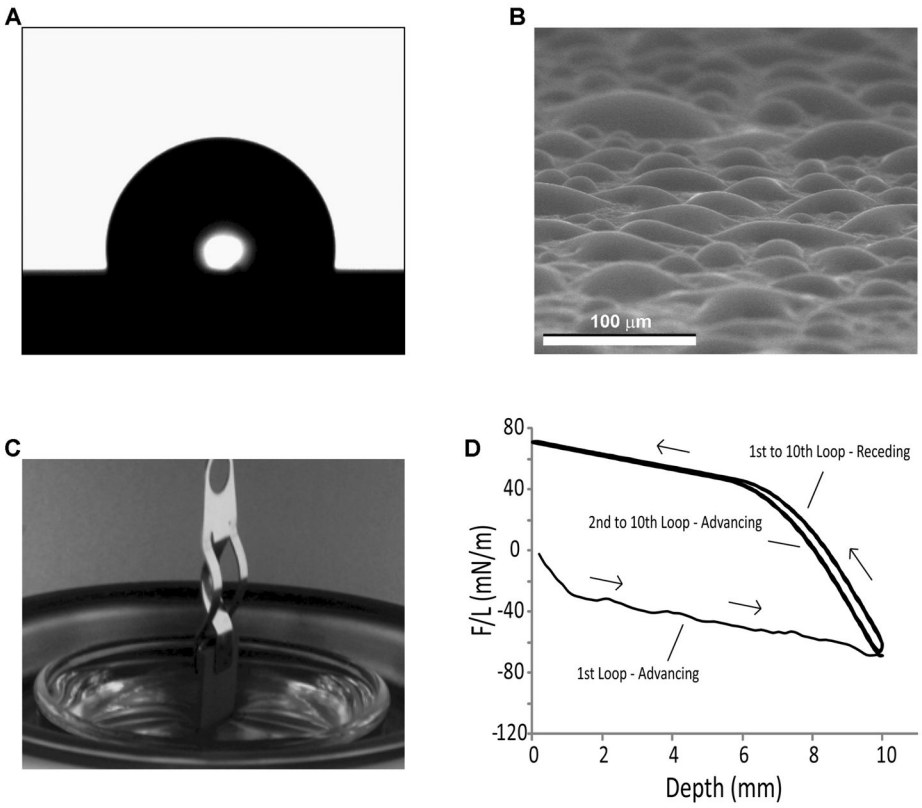

Figure 1.

Static and dynamic evaluations of surface wettability. (A) Micrograph of a sessile water drop used to measure contact angles. (B) ESEM image of the condensation of water on the surface of Ti specimens for contact angle assessment. (C) Photograph of the Wilhelmy plate setup revealing the use of a tensiometer to suspend a rectangular Ti specimen that is partially immersed in a water reservoir. (D) Example of a typical DCA 10-loop hysteresis cycle, showing the advancing and receding curves.

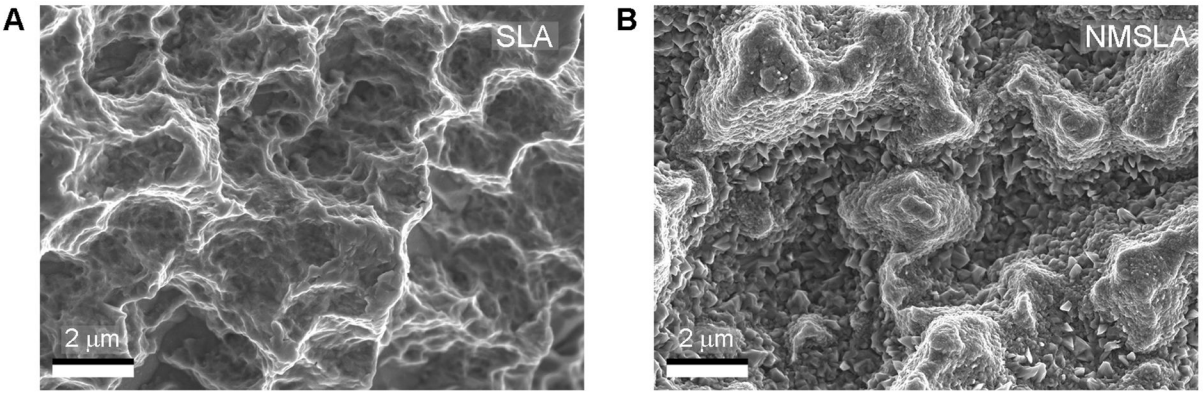

Figure 2.
SE images of (A) microrough Ti specimens (SLA) and (B) microrough specimens that were subsequently heat-treated to superimpose oxidation-induced nanostructures on the surface (NMSLA). SLA surfaces possessed peaks and valleys in the order of tens of micrometers as a result of the sandblasting process, with some sharp sub-microscale features left from the acid-etch treatment. After the nanomodification oxidation treatment for 90 minutes at 740 °C in flowing synthetic air, the NMSLA surfaces possessed high and homogeneous concentrations of nanostructures.

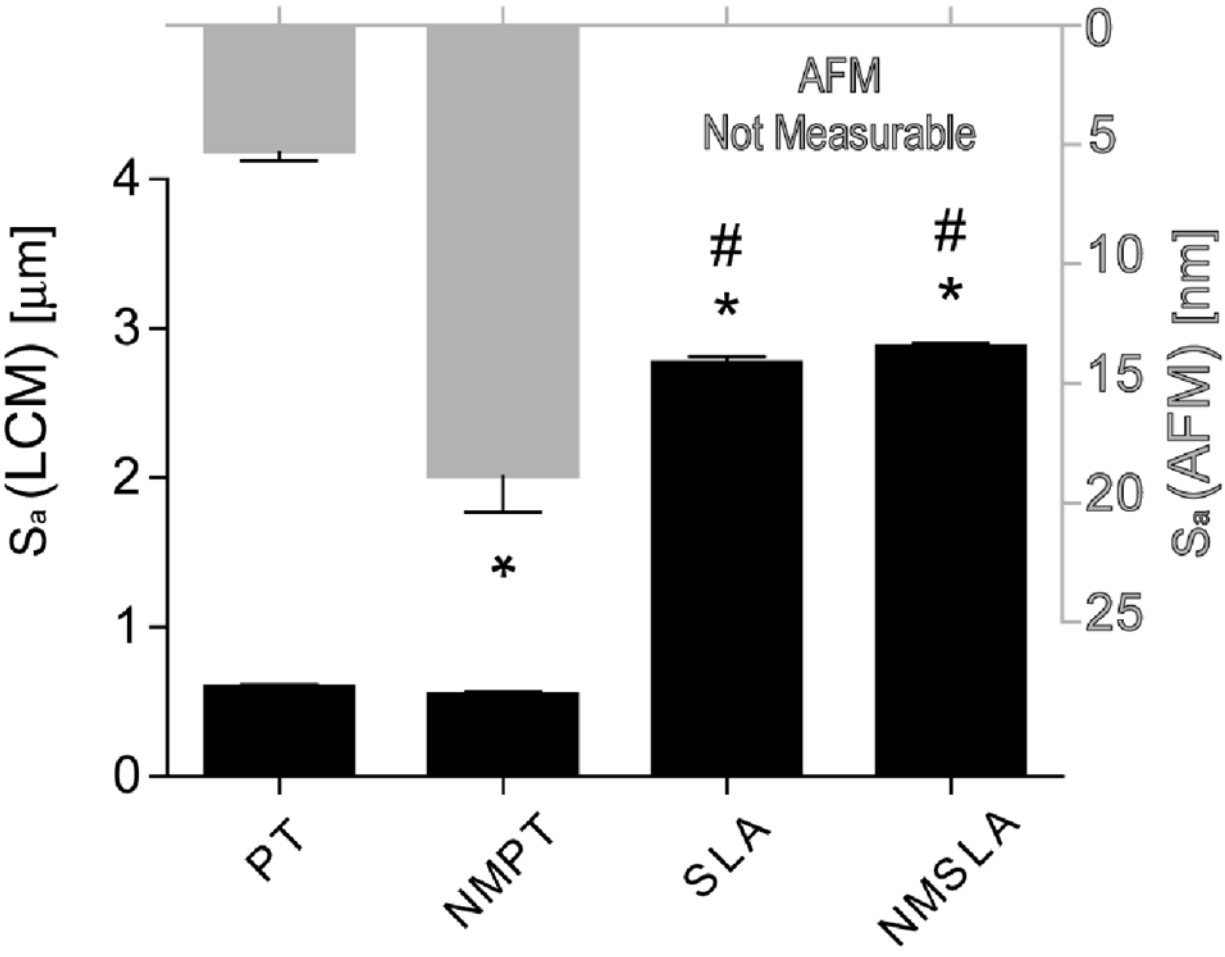

Figure 3.

Average surface roughness (S_a) values of original and nanomodified surfaces measured by laser confocal microscopy (LCM, black bars) and atomic force microscopy (AFM, grey bars). AFM scans were not possible on microrough SLA and NMSLA specimens, due to z-height tool limitations, thus requiring the evaluation of microsmooth PT and NMPT specimens. * refers to a statistically-significant p value below 0.05 vs. PT; # refers to a statistically-significant p value below 0.05 vs. NMPT.

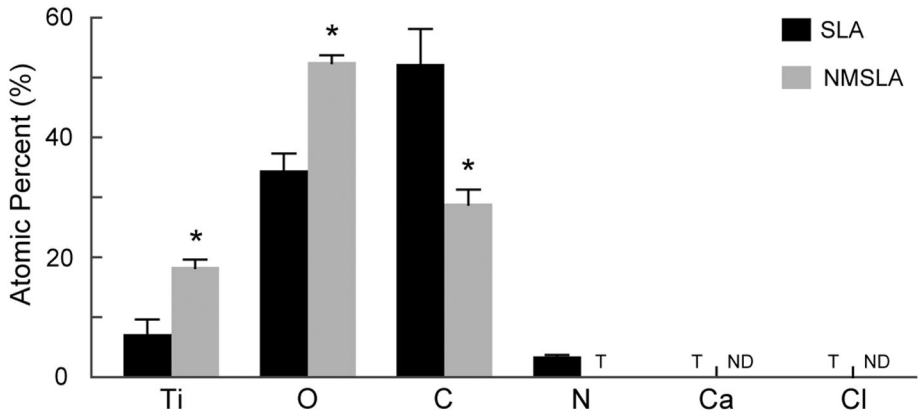

Figure 4.

Surface elemental compositions of the SLA and NMSLA specimens measured by XPS. All surfaces were mainly composed of Ti, O and C. N was also present at low levels on the SLA surfaces, while NMSLA surfaces only had traces (T) of N. Traces of other contaminants such as Ca and Cl were found on the surface of SLA specimens, but these were not detectable (ND) on the NMSLA surfaces. * refers to a statistically-significant p value below 0.05 vs. SLA.

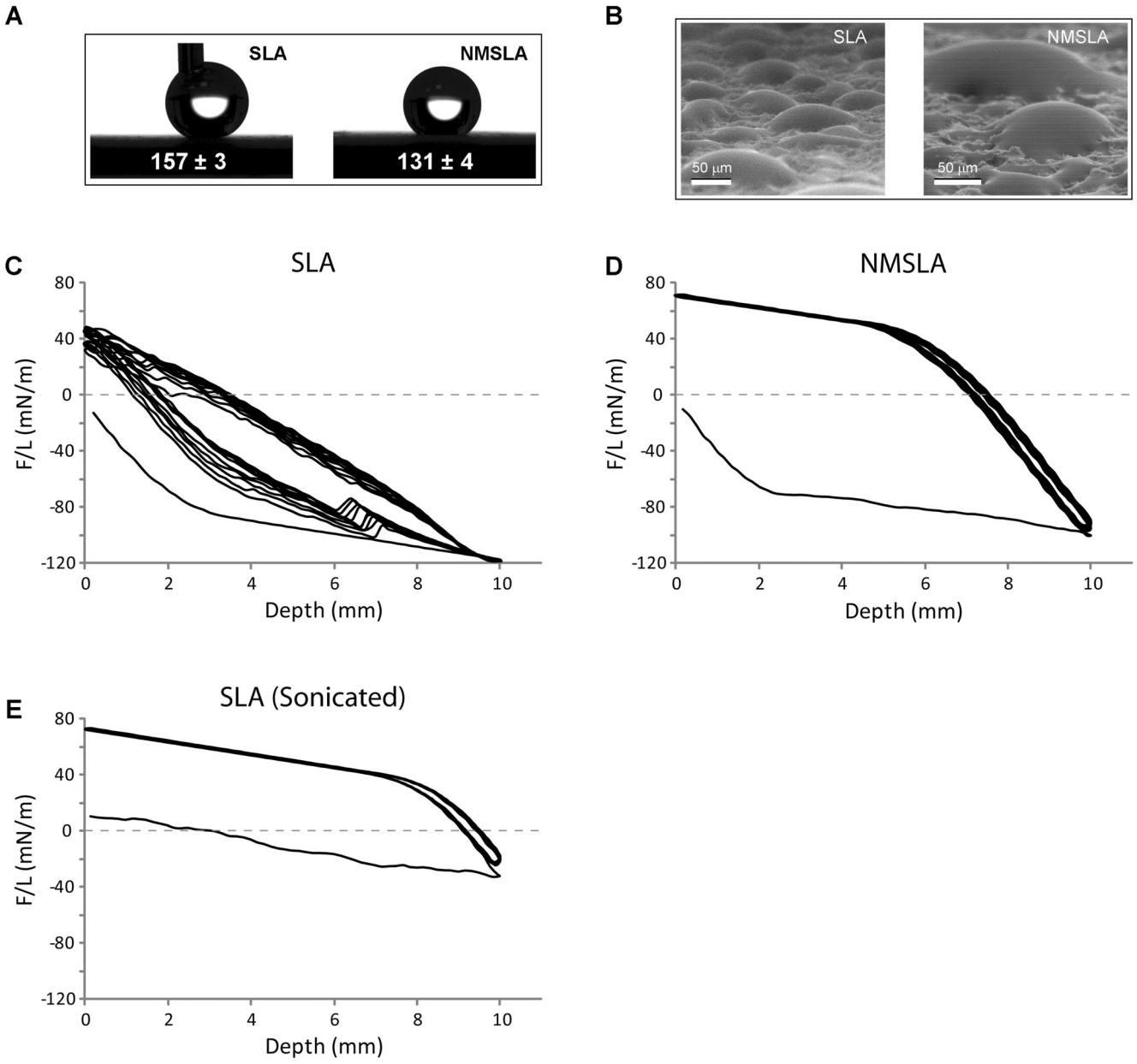

Figure 5.

Static and dynamic contact angle analyses on SLA and NMSLA specimens. (A) Optical sessile-drop water contact observations on the surfaces of SLA and NMSLA specimens showed hydrophobic static responses. (B) ESEM image showing condensed water droplets on the surfaces of SLA and NMSLA specimens for contact angle evaluations. Some of the smaller droplets exhibited complete wetting of the surface. (C–D) Force graphs of 10-loop Wilhelmy experiments showed extremely negative F/L values for the initial advancing loop of (C) SLA and (D) NMSLA specimens. Subsequent immersion-emersion loops on the SLA specimens continued to show negative values without reaching equilibrium. In contrast, NMSLA specimens presented positive F/L values for all following loops without evidence of appreciable hysteresis. (E) Sterilized SLA specimens were ultrasonically cleaned after

dynamic contact angle analysis and reanalyzed, showing a slightly negative F/L value for the initial loop and positive values for the subsequent loops without appreciable hysteresis.

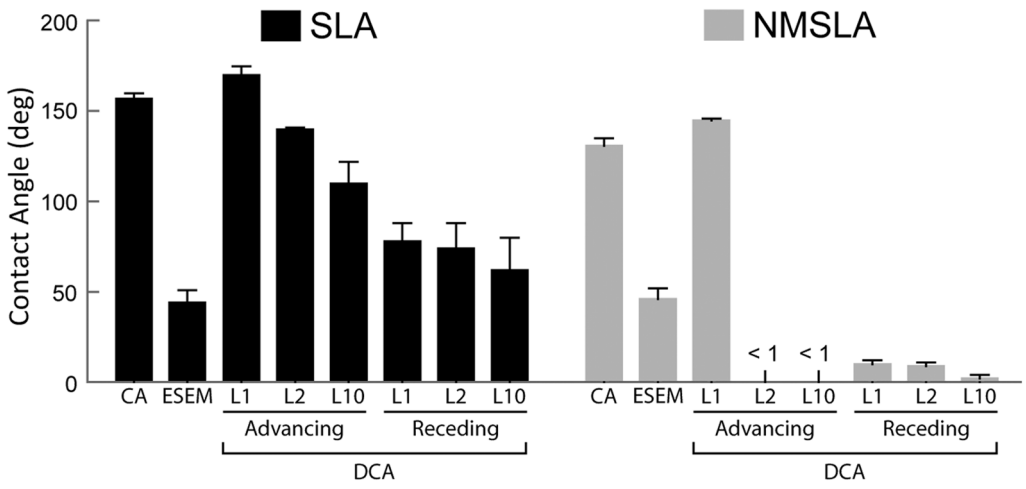

Figure 6.

Contact angles measured by sessile-drop technique (CA), ESEM, or calculated from the measured F/L values from different advancing and receding loops (L) from dynamic analyses of the autoclaved SLA and NMSLA specimens.

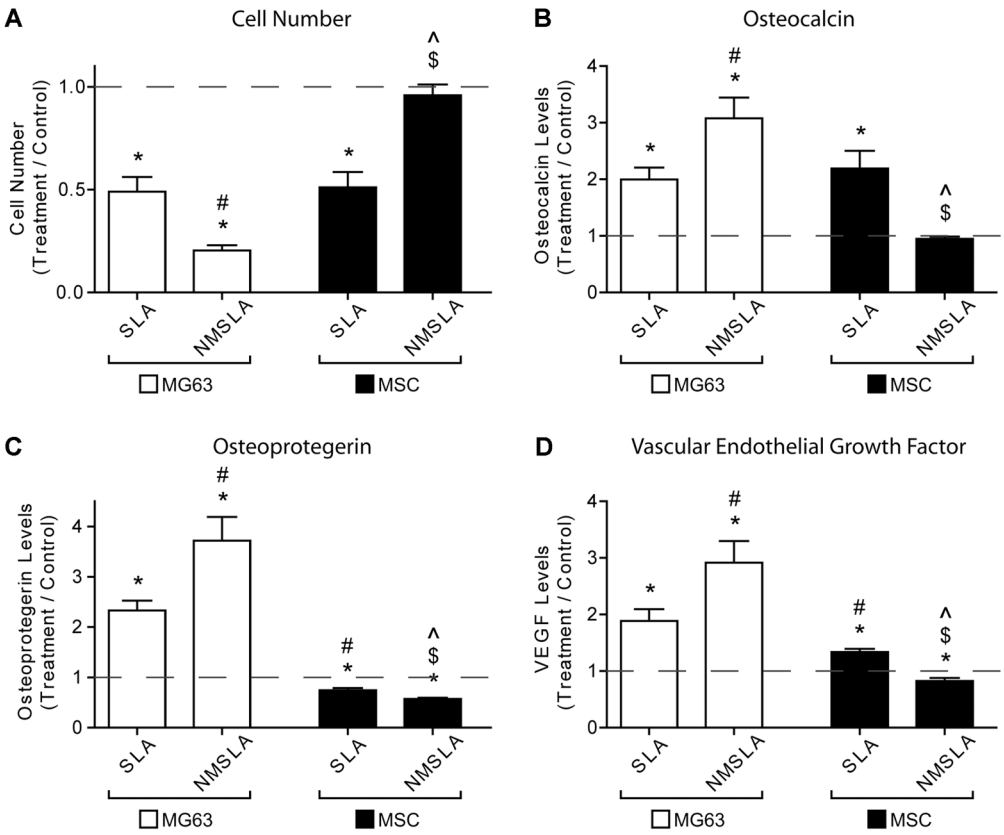

Figure 7.

Effects of micro and nanoscale surface modifications on immature MG63 osteoblast-like cells and human MSCs relative to microsmooth PT controls (dashed line). Osteoblasts and MSCs were plated on PT controls, SLA, and NMSLA surfaces and grown to confluence. The nanomodification involves surface oxidation in flowing synthetic air for 90 minutes at 740 °C. At confluence, (A) cell number, (B) osteocalcin, (C) osteoprotegerin, and (D) VEGF levels were measured. Data represented are the mean ± SE of six independent samples. * refers to a statistically-significant p value below 0.05 vs. PT; # refers to a statistically-significant p value below 0.05 vs. SLA-MG63; $ refers to a statistically-significant p value below 0.05 vs. NMSLA-MG63; ^ refers to a statistically-significant p value below 0.05 vs. SLA-MSC.